Enhanced Permeability of Charged Dendrimers across Tense Lipid Bilayer Membranes

Li-Tang Yan[†,*] and Xiaobo Yu[‡]

[†]Physikalische Chemie II, Universität Bayreuth, D-95440 Bayreuth, Germany, and [‡]Biochemistry Department, NMI Natural and Medical Sciences Institute at the University of Tuebingen, 72770 Reutlingen, Germany

ABSTRACT Dendrimers have successfully proved themselves as functional nanodevices for drug delivery because they can render drug molecules a greater water solubility, bioavailability, and biocompatibility. It has recently been suggested that the structural changes of cell membranes (*e.g.*, local lipid density and actual pore or hole) could affect the permeability across them for dendrimers. However, to understand these effects requires direct measurements in a single cell and is thus very difficult and more challenging. Here we use mesoscopic simulations to investigate the tension-mediated complexes comprising charged dendrimers and lipid bilayer membranes. The structures of membranes are alternated by adjusting their surface tensions. Our simulations demonstrate that the permeability of charged dendrimers can be effectively enhanced in the tense membranes, and the permeability in the actual hole is several times higher than that in the lipid-poor section. The possible mechanism of charged dendrimer-induced pore nucleation in the tense membranes is evaluated. The findings have implications in tuning intracellular delivery rates and amounts in nanoscale complex and chemotherapeutics.

KEYWORDS: tense bilayer membrane · dendrimer · complex · enhanced permeability · cytotoxicity

Understanding the interactions of nanoparticles with biological membranes is of fundamental importance in determining their potential application as drug delivery vehicles and therapeutic agents. As a framework in multifunctional nanodevices, dendrimers are particularly useful in the development of targeted chemotherapeutic agents.[1−3] Recently, the pharmaceutical applications of dendrimers have been extended to delivery systems for drugs, particularly, the nonsteroidal anti-inflammatory, antimicrobial/antiviral, and potent anticancer drugs.[3] As dendrimers approach a living animal cell, one of the most important interactions is with the cellular plasma membranes which form the basis of many important cellular organelles, such as the endoplasmic reticulum, the Golgi apparatus, or the vesicular transport system.[4−6] Thereby a more thorough understanding of the interactions between dendrimers and lipids will address many relevant issues pertaining to real cells because lipids are the most prevalent component of plasma membrane.

Lipid bilayer models have been shown to give qualitatively accurate predictions for *in vivo* cell studies in regards to membrane fusion and vesiculation.[7−9] Typically, the lipid bilayer membranes will stretch in response to external forces, which could create a localized region that is lipid-poor. Above a critical force, the lipid bilayer membranes will split open and form pores.[4−6,10−12] It has been suggested that these structural changes of the lipid bilayer membranes could affect the permeability of the solvent or chemotherapeutic agents.[3] Understanding the detailed influence of these structural changes of membranes on the permeability is of great importance for gene and targeted drug deliveries and the development of cell transfection agents. However, the direct measurement for the effect in a single cell is very difficult and is thus more challenging.[3]

When experiments encounter difficulties, tailored computer simulations offer an alternative approach, with their unique ability to identify and separate individual contributions to the phenomenon or process of interest. To carry out this study, we use a mesoscopic simulation technique, dissipative particle dynamics (DPD).[13] For the complicated problem considered here, DPD offers an approach that can be used for modeling physical phenomena occurring at larger time and spatial scales than some other classic methods as it utilizes a momentum-conserving thermostat and soft repulsive interactions between the beads representing clusters of molecules. The method can reproduce the correct hydrodynamic forces appropriate to a fluid and has proven to be especially useful in

*Address correspondence to li-tang.yan@uni-bayreuth.de.

Received for review April 28, 2009 and accepted June 30, 2009.

Published online July 7, 2009.
10.1021/nn9004236 CCC: $40.75

studying the mesoscopic behaviors of lipid membranes.[14−18] A key difference in the simulation method between our simulations and the simulations cited above is the fact that the Coulombic interactions among the charged beads (*i.e.*, the head beads of the lipid, the terminal beads of dendrimers, and the explicit counterions) are considered in the present simulations. Actually, the electrostatic interactions have been proved to influence the membrane structures and the interactions between lipid bilayer membranes and ionizable chains due to the counterion condensation and the interactions between the counterions and the charged groups (see refs 19 and 20 and Supporting Information Figure S4).

Here, the lipid density of the bilayer membrane is changed by applying external force (stretching the membrane). Then the charged dendrimer is added into the system and interacts with the bilayer membrane of various lipid densities and surface tensions. Our simulations will demonstrate that the charged dendrimer can induce the hole formation in the membrane with enough tension. Consequently, the influence of membrane structures, including the lipid-poor section and actual pore or hole, on the permeability of the charged dendrimer can be examined. The possible mechanism of charged dendrimer-induced pore nucleation in the tense membranes will also be discussed. To the best our knowledge, this is the first study for the tension-mediated complexes comprising charged dendrimers and lipid bilayer membranes.

Full technical details on the models of the lipid and the charged dendrimer can be found in Supporting Information. Briefly, each amphiphilic lipid consists of a headgroup and two tails (see Supporting Information Figure S1A). The headgroup contains three connected hydrophilic beads, and the top two of them carry the charges of +1 and −1. Each tail includes three connected hydrophobic beads. This model of lipid may be related to the dipalmitoylphosphatidylcholine (DPPC) molecule. For this purpose, three function groups are lumped together into one bead. The model of charged dendrimer is mapped from the structure of the polyamidoamine (PAMAM) dendrimer (see Supporting Information Figure S1B). Only the terminal beads of the dendrimer model are hydrophilic and carry the charge of +1. The other moiety of the dendrimer is uncharged and hydrophobic. Solvent particles are represented by a single bead. At the beginning of our simulations, a stable, tensionless square bilayer membrane that is in the fluid state and consists of 1054 lipids is obtained first (see Supporting Information Figure S2). The area per lipid, A_l, of this membrane is about $1.28r_c^2$ where r_c (about 0.7 nm) is the truncated distance of the conservative force in the DPD model. Consequently, the side length of the tensionless square bilayer membrane is 18 nm. A_l and the membrane tension can be increased by stretching the membrane (see Support Information 2).

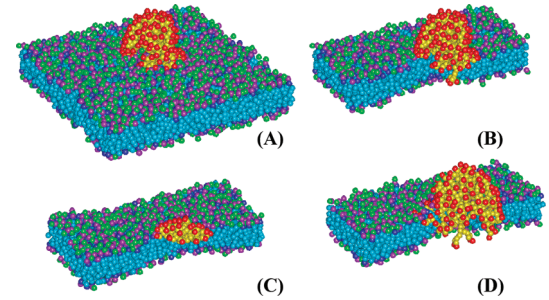

Figure 1. Complexes between tensionless bilayer membranes and charged dendrimers. The bilayer membrane patches, of linear extent 18 nm, contains 1054 lipids. The area per lipid is about $1.28r_c^2$. The time for each simulation snapshot is 15 μs. (B−D) Cross-sectional views along the dendrimers revealing the distribution of the dendrimer beads inside the membranes. (A,B) Complex of the bilayer membrane with a G5 dendrimer where the interaction parameter between the beads of lipid tails and uncharged dendrimer beads, α_{TU}, is 28. (C) Complex between the bilayer membrane and a G3 dendrimer with the same α_{TU}. (D) Cross-sectional view of the bilayer membrane−G5 dendrimer complex with a stronger attraction between the beads of lipid tails and the uncharged dendrimer beads (*i.e.*, α_{TU} = 15). Solvent and counterions are not shown for clarity. Color scheme: head beads with positive charge (green), head beads with negative charge (pink), head beads without charge (blue), tail beads (cyan), charged beads of dendrimer (red), and uncharged beads of dendrimer (yellow).

The charged dendrimers with various generations (*i.e.*, generation 3 (G3), generation 5 (G5), and generation 7 (G7)) are used in the simulations, and their equilibrated radii of gyration R_g are comparable to the experimental or simulated results of PAMAM dendrimers (see Supporting Information Figure S3 and Table S2). An equilibrium dendrimer then can be added to the lipid bilayer membrane system in which the lowest beads of the dendrimer are adjacent to the top surface of the membrane.[11] To preserve charge neutrality, the randomly selected solvent beads are changed into the counterions of a charge of −1 in the membrane system.

RESULTS AND DISCUSSION

Previous experiments demonstrated that the charged G3 PAMAM dendrimer is only attracted to the edge of the lipid bilayer membrane but cannot induce defects, whereas the charged PAMAM G5 dendrimer is prone to cause the formation of a pore in the membrane.[3−5] We thus start our complex protocol by assembling charged G3 and G5 dendrimers and a tensionless bilayer membrane, where a lightly repelled interaction between the beads of lipid tails and uncharged dendrimer beads (*i.e.*, α_{TU} = 28) is used. The detailed process and equilibrated structure for the complexes are shown in Figure 1A−C and Supporting Information Video 1. During the assembling process, the G5 dendrimer gradually inserts into the membrane and leads to the formation of a small pore in it. However, the G3 dendrimer only rests on one side of the membrane and causes almost no defect. The simulations reproduce experimental results showing that the size of

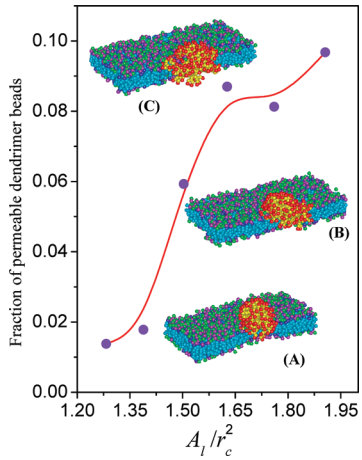

Figure 2. Permeability of the charged G5 dendrimers across the tense lipid bilayer membranes. The solid circles plot the fraction of the permeable dendrimer against the area per lipid molecular A_l (corresponding to the surface tensions of the membranes). The red line is used only to guide the eyes. The permeable dendrimer beads are defined as the dendrimer beads beyond the middle or reach the other side of the bilayer membrane during the simulation period (15 μs). The areas per lipid for the cross-sectional views of the snapshots are $1.39r_c^2$ (A), $1.50r_c^2$ (B), and $1.63r_c^2$ (C). All data points, including the plot and the snapshots, are obtained at 15 μs. The interaction parameter between the beads of lipid tails and uncharged dendrimer beads, α_{TU}, is 28. The lipid number and color code for the complexes are the same as those in Figure 1. Solvent and counterions are not shown for clarity.

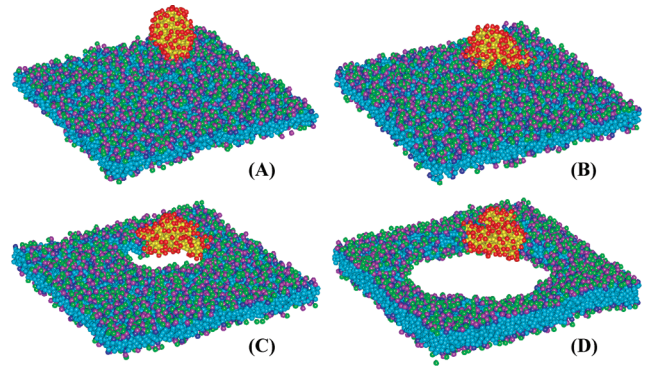

Figure 3. Dendrimer-induced hole in the tense bilayer membrane. The area per lipid molecular for the membrane is $A_l = 2.06r_c^2$ at the initial time. A charged G5 dendrimer is used in the simulation. The time for each snapshot is 0 μs (A), 4.5 μs (B), 6.9 μs (C), and 15 μs (D). The interaction parameter between the beads of lipid tails and uncharged dendrimer beads, α_{TU}, is 28. The lipid number and color code for the complexes are the same as those in Figure 1. Solvent and counterions are not shown for clarity.

the dendrimer plays an important role in pore formation.[3−5] To further examine the mechanism of charged dendrimer-induced pore nucleation in the tense membrane (see Figure 5 and its corresponding analysis), a reduced interaction parameter between the beads of lipid tails and uncharged dendrimer beads (*i.e.*, $\alpha_{TU} = 15$) is also selected, which can give a more complete complex between the dendrimer and the tensionless lipid bilayer membrane (see Figure 1D).

Although the G5 dendrimer can cause the formation of a pore in the tensionless membrane, only a few dendrimer beads can penetrate across the lipid bilayer membrane and the pore size is very small (see Figure 1B and Supporting Information Video 1). The experimental results suggested that the change of the lipid density in the membrane could affect the permeability of the dendrimers.[3−5] In our simulations, the lipid density is controlled by stretching the membrane. Consequently, the surface tension of the bilayer membrane will be changed during this stretching. Here the parameter of A_l (*i.e.*, the area per lipid) is used to denote the lipid density. The relation between A_l and the surface tension of the lipid bilayer membrane can be found in Figure 5D.

The charged G5 dendrimer is added into the systems of the lipid bilayer membranes with different surface tensions, and then each system is equilibrated over 15 μs. The cross-sectional snapshots in Figure 2 show the equilibrated structures of the complexes at different A_l. Clearly, more dendrimer beads penetrate into the bilayer membranes with the increasing surface tension or A_l. Note that, within the scale of A_l in Figure 2, not only the hole with bigger size but also the rupture does not take place in the lipid bilayer membranes. To further analyze the dependence of the dendrimer penetrability on the lipid density, we quantify the penetrability of the dendrimer by the fraction of permeable dendrimer beads. Here the permeable dendrimer beads are defined as the dendrimer beads beyond the middle or reach the other side of the bilayer membrane during the simulation period (15 μs). The solid circles and red line in Figure 2 show the quantitative relation between the fraction of permeable dendrimer beads and A_l. The fraction of permeable dendrimer beads increases from 0.014 to 0.097 when the area per lipid is changed from $1.28r_c^2$ to $1.91r_c^2$. These results reveal that the localized lipid-poor region in the lipid bilayer membrane will be in possession of high permeability, verifyinging the suggestion from previous experiments.[3−5] Owing to minimizing the energy of the system, the charged dendrimer beads tend to exhibit a balanced distribution in both surfaces of the bilayer membrane. The sparse lipids in the lipid-poor region provide more space for the diffusion of the dendrimer beads across the bilayer membrane to realize this balanced distribution.

The behavior of the complex changes completely when the charged G5 dendrimer is placed on a lipid bilayer membrane with a higher surface tension ($A_l > 1.95r_c^2$). As an example, Figure 3 and Supporting Information Video 2 show a detailed process about the complex between the charged G5 dendrimer and a tense bilayer membrane with initial $A_l = 2.06r_c^2$. We observe the rupture of the membrane and the formation of a big hole at about 6.5 μs. To further confirm whether the rupture of the membrane is induced by the charged dendrimer or it is a consequence just from the stretching, the full tension histories of the complex and a

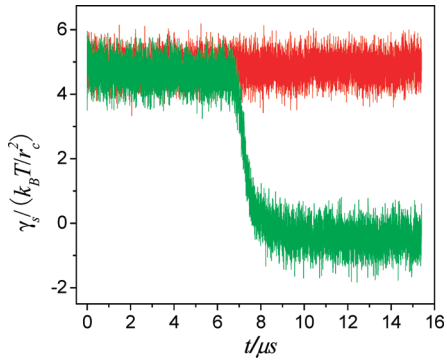

Figure 4. Full histories of the surface tensions γ_s. (Red line) the single tense membrane with initial $A_l = 2.06r_c^2$. (Green line) the complex between the charged G5 dendrimer and the tense membrane with the same initial A_l. The interaction parameter between the beads of lipid tails and uncharged dendrimer beads, α_{TU}, is 28. The lipid number is the same as those in Figure 1.

single lipid bilayer membrane with the same initial tension are illustrated in Figure 4. An abrupt crossover occurs in the curve of the complex. Then the stress of the complex is rapidly released, corresponding to the big hole formation and the rupture of the bilayer membrane. Nevertheless, the tension curve of the single membrane is of only a light fluctuation around 4.82 k_BT/r_c^2 during the whole period, indicating the integrity of the membrane. The comparison implies that the charged dendrimer indeed plays an important role in the big hole formation of the tense bilayer membrane.

Supporting Information Video 2 and Figure 3C,D show that more dendrimer beads diffuse to the other side of the membrane once the hole forms in the lipid bilayer membrane. Simultaneously, the dendrimer attaches to the edge of the hole. A quantitative analysis shows that the fraction of permeable dendrimer beads in Figure 3D is about 0.35. Compared with the result at $A_l = 1.91r_c^2$, there is about 2.6 times increase for the permeable dendrimer beads. Clearly, a great difference occurs between the permeability in the lipid-poor section and that in the actual hole. Our simulations may give a quantitative basis for discerning these two sections in the cell by different methods, such as enzymatic leakage assays. However, the bilayer membrane simulated here seems to be more stretchable than the real phospholipid bilayers because they also contain protein and cholesterol. Thus, the simulation results should be calibrated according to the maximal A_l from simulations and experimental observations if they are applied to the real phospholipid bilayers.

To gain insight into the charged dendrimer-induced hole formation in the tense bilayer membrane, we focus on the mechanism of incipient pore nucleation that directly causes the rupture of the membrane. Three charged dendrimers (G3, G5, and G7) and the tensionless bilayer membranes are first assembled over 15 μs. Here, the interaction parameter α_{TU} is set to 15 with which more complete complexes can be realized (see Figure 1D). These complexes are then stretched until the membranes rupture. Figure 5 shows the corresponding surface tension curves and the snapshots of the complexes at the critical point where membrane fails. Also, a detailed process of the complex between a charged G7 dendrimer and the bilayer membrane is given in Supporting Information Video 3. As illustrated in Figure 5, all incipient pores occur in the positions away from the dendrimer in the G3 dendrimer−membrane complex. In the G5 dendrimer−membrane complex, the pore at the edge of the dendrimer appears only a little later than those away from the dendrimer. However, all pores initially form along the edge of the dendrimer in the G7 dendrimer−membrane complex.

A high surface tension is usually required for the pore nucleation in a bilayer membrane because the pore nucleation is an activated process and the spontaneous forma-

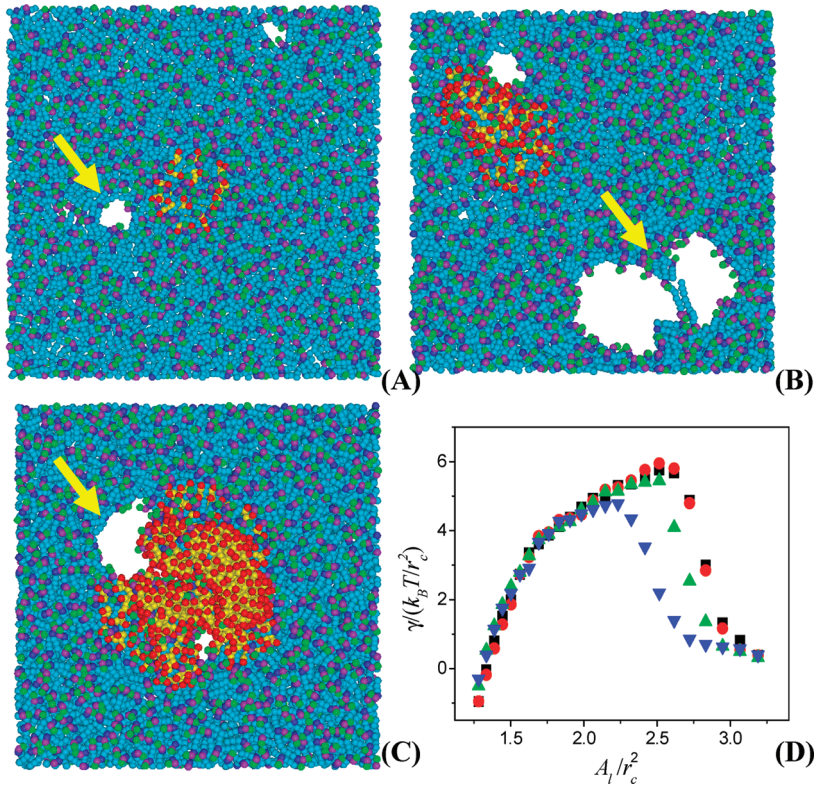

Figure 5. Incipient pores in the complexes between the charged dendrimer and the lipid bilayer membrane. The dendrimer generations are G3 (A), G5 (B), and G7 (C), where the interaction parameter between the beads of lipid tails and uncharged dendrimer beads, α_{TU}, is 15. The areas of single lipid, A_l, are $2.63r_c^2$ (A and B) and $2.15r_c^2$ (C). The lipid number and color code for the complexes are the same as those in Figure 1. Solvent and counterions are not shown for clarity. The yellow arrows indicate the initial pores in the membranes. (D) Corresponding surface tension as functions of the area per lipid for the complexes composed of the bilayer membrane and G3 (red circles), G5 (green triangles), and G7 (blue triangles) dendrimers. The plot of black squares corresponds to the tension curve of the single membrane. The error for each curve is about $\pm 0.33k_BT/r_c^2$.

tion of pore nuclei in a moderately stretched membrane is scarce.[10] Our simulations indicate that the presence of the charged dendrimer is helpful to invoke this activity or the dendrimer can induce a pore nucleation at a low surface tension. However, the G3 dendrimer is not able to nucleate pores within the bilayer membrane. This revels that there is also an energy barrier which prevents the spontaneous formation of the pore nucleation induced by the dendrimer. The curves in Figure 5D show that the critical surface tension of the membrane rupture decreases with the increasing dendrimer generation, demonstrating that the localized membrane with the bigger dendrimer more easily overcomes the energy barrier. Compared to the G3 dendrimer, more beads of G5 and G7 dendrimers will diffuse into the bilayer membrane, which disrupt the ordered lipid arrangement and consequently weaken the energy barrier. Moreover, once the pore nucleation forms in the bilayer membrane, the growth and closure of the pore are controlled by the competition between the surface tension of the membrane and the line tension associated with the rim of the pore.[10] The bigger pore nucleation induced by the G7 dendrimer is of a smaller line tension, consequently leading to a lower tolerance of the membrane and the hole formation at a lower surface tension.[23]

CONCLUSIONS

By employing a mesoscopic method, we investigate the tension-mediated complexes between charged dendrimers and lipid bilayer membranes. A distinguished (and unique) feature of this study is that the difference between the permeability in the actual hole and that in the lipid-poor section for the charged dendrimers is presented. We find that the permeability of charged dendrimers can be effectively enhanced in the tense membranes, and the permeability in the actual hole is several times higher than that in the lipid-poor section. Our simulations also provide insight into the possible mechanism of charged dendrimer-induced pore nucleation in the tense membranes. The strutures of the lipid bilayer membrane can be altered by not just an external force but also the surroundings (*e.g.*, temperature, pH, or salt concentration). Thus, this research should have contributions to improve the design of dendrimers in medical application. Looking to the future, the findings have a bearing on understanding the complexes between the charged dendrimers (or other nanoparticles) and the cell membrane, which is a subject of interest for improving drug and gene delivery vehicles, developing new cell transfection agents and predicting the cytotoxicity of different charged nanoparticles.

METHODS

We use the DPD technique, which is a coarse-grained molecular dynamics (MD) approach.[13] DPD utilizes a momentum-conserving thermostat and soft repulsive interactions between the beads representing clusters of molecules and thus can capture the hydrodynamics of complex fluids and can model physical phenomena occurring at larger time and spatial scales. The present simulations are carried out using five different interaction forces between beads, such as the conservative interaction force F^C, dissipative force F^D, random force F^R, bond force F^S (including harmonic bond force and bond angle force), and the electrostatic force F^E (*i.e.*, $f_i = \sum_{j\neq i}(F_{ij}^C + F_{ij}^D + F_{ij}^R + F_{ij}^S + F_{ij}^E)$, where the sum runs over all beads j. These forces, excluding the electrostatic one, are pairwise additive and depend on the coordinate differences. F^C, F^D, and F^R are of short-range with a fixed cutoff distance r_c. The electrostatic force F_i^E is analyzed based on a modification particle−particle−particle−mesh (P3M) algorithm.[21] The detailed forms of these forces can be found in Supporting Information 1. Similar to MD simulations, DPD captures the time evolution of a many-body system through the numerical integration of Newton's equation of motion. Here, we use a modified velocity−Verlet algorithm due to Groot and Warren[13] to solve the motion equation. In the simulations, the radius of interaction, the bead mass, and the temperature are set as the unit. A characteristic time scale is then defined as $\tau = \sqrt{mr_c^2/k_BT}$. Our simulation box is $(26r_c)^3$ in size and with periodic boundary condition in all directions. A bead number density of $3/r_c^3$ is selected. The time step of $\Delta t = 0.02\tau$ is set, which assures the accurate temperature control of the simulation system.[22]

The typical area per lipid in a tensionless DPPC membrane is about 0.64 nm^2.[14] We use this value to estimate the physical length of our simulations and find that r_c is about 0.7 nm. Thereby, the area of the tensionless membrane in our simulation is 18 nm × 18 nm. The time unit τ is related to the physical time by comparing the in-plane diffusion coefficient of lipids. A typical experimental result of this coefficient is 5 μm^2/s.[16] Equating this value to the simulation result yields $\tau = 7.7$ ns, and thus the total physical time of each calculation is about 15 μs (10^5 time steps).

Acknowledgment. We would like to thank Dr. Markus Müller and Dr. Youyong Xu for their help on the calculation and valuable discussion. L.-T.Y. acknowledges the hospitality of Prof. Alexander Böker and Prof. Andreas Fery at the University of Bayreuth. The financial support from Alexander von Humboldt Foundation is greatly appreciated.

Supporting Information Available: Detailed forms of forces used in the DPD model. The DPD models of lipid and dendrimer molecules. Additional simulation results and videos. This material is available free of charge *via* the Internet at http://pubs.acs.org.

REFERENCES AND NOTES

1. Langer, R. Drug Delivery and Targeting. *Nature* **1998**, *392*, 5–10.
2. Tomalia, D. A. Birth of a New Macromolecular Architecture: Dendrimers as Quantized Building Blocks for Nanoscale Synthetic Polymer Chemistry. *Prog. Polym. Sci.* **2005**, *30*, 294–324.
3. Leroueil, P. R.; Hong, S.; Mecke, A.; Baker, J. R.; Orr, B. G.; Banaszak Holl, M. M. Nanoparticles Interaction with Biological Membranes: Does Nanotechnology Present a Janus Face. *Acc. Chem. Res.* **2007**, *40*, 335–342.
4. Hong, S.; Leroueil, P. R.; Janus, E. K.; Peters, J. L.; Kober, M. M.; Islam, M. T.; Orr, B. G.; Baker, J. R.; Banaszak Holl, M. M. the Interaction of Polyamidoamine (PAMAM) Dendrimers with Supported Lipid Bilayers and Cells: Nanoscale Hole Formation and Enhanced Membrane Permeability. *Bioconjugate Chem.* **2006**, *17*, 728–734.
5. Landmark, K. J.; DiMaggio, S.; Ward, J.; Kelly, C.; Vogt, S.; Hong, S.; Kotlyar, A.; Myc, A.; Thomas, T. P.; Penner-Hahn,

J. E.; Baker, J. R.; Banaszak Holl, M. M.; Orr, B. G. Synthesis, Characterization, and *In Vitro* Testing of Superparamagnetic Iron Oxide Nanoparticles Targeted Using Folic Acid-Conjugated Dendrimers. *ACS Nano* **2008**, *2*, 773–783.
6. Kuokowska-Latallo, J. F.; Bielinska, A. U.; Johnson, J.; Spindler, R.; Tomalia, D. A.; Baker, J. R. Efficient Transfer of Genetic Material into Mammalian Cells Using Starburst Polyamidoamine Dendrimers. *Proc. Natl. Acad. Sci. U.S.A.* **1996**, *93*, 4897–4902.
7. Marrink, S. J.; Mark, A. E. the Mechanism of Vesicle Fusion As Revealed by Molecular Dynamic Simulations. *J. Am. Chem. Soc.* **2003**, *125*, 11144–11145.
8. Reynwar, B. J.; Iiiya, G.; Harmandaris, V. A.; Müller, M. M.; Kremer, K.; Deserno, M. Aggregaion and Vesiculation of Membrane Proteins by Curvature-Mediated Interactions. *Nature* **2007**, *447*, 461–464.
9. Qiao, R.; Roberts, A. P.; Mount, A. S.; Klaine, S. J; Ke, P. C. Translocation of C_{60} and Its Derivatives across a Lipid Bilayer. *Nano Lett.* **2007**, *7*, 615–619.
10. Wang, Z. J.; Frenkel, D. Pore Nucleation in Mechanically Stretched Bilayer Membranes. *J. Chem. Phys.* **2005**, *123*, 154701.
11. Lee, H.; Larson, R. G. Molecular Dynamics Simulations of PAMAM Dendrimer-Induced Pore Formation in DPPC Bilayers with a Coarse-Grained Model. *J. Phys. Chem. B* **2006**, *110*, 18204–18211.
12. Kelly, C. V.; Leroueil, P. R.; Nett, E. K.; Wereszczynski, J. M.; Baker, J. R.; Orr, B. G.; Banaszak Holl, M. M.; Andricioaei, I. Poly(amidoamine) Dendrimers on Lipid Bilayers I: Free Energy and Conformation of Binding. *J. Phys. Chem. B* **2008**, *112*, 9337–9345.
13. Groot, R. D.; Warren, P. B. Dissipative Particle Dynamics: Bridging the Gap between Atomistic and Mesoscopic Simulation. *J. Chem. Phys.* **1997**, *107*, 4423–4435.
14. Smith, K. A.; Jasnow, D.; Balazs, A. C. Designing Synthetic Vesicles That Engulf Nanoparticles. *J. Chem. Phys.* **2007**, *127*, 084703.
15. Shillcock, J. C.; Lipowsky, R. Equilibrium Structure and Lateral Stress Distribution of Amphiphilic Bilayers from Dissipative Particle Dynamics. *J. Chem. Phys.* **2002**, *117*, 5048–5061.
16. Shillcock, J. C.; Lipowsky, R. Tension-Induced Fusion of Bilayer Membranes and Vesicles. *Nat. Mater.* **2005**, *4*, 225–228.
17. Alexeev, A.; Uspal, W. E.; Balazs, A. C. Harnessing Janus Nanoparticles to Create Controllable Pores in Membranes. *ACS Nano* **2008**, *2*, 1117–1122.
18. Laradji, M.; Sunil Kumar, P. B. Dynamics of Domain Growth in Self-Assembled Fluid Vesicles. *Phys. Rev. Lett.* **2004**, *93*, 198105.
19. Tieleman, D. P.; Leontiadou, H.; Mark, A. E.; Marrink, S. J. Simulation of Pore Formation in Lipid Bilayers by Mechanical Stress and Electrical Fields. *J. Am. Chem. Soc.* **2003**, *125*, 6382–6383.
20. Li, L.; Vorobyov, I.; Allen, T. W. Potential of Mean Force and pK_a Profile Calculation for a Lipid Membrane-Exposed Arginine Side Chain. *J. Phys. Chem. B* **2008**, *112*, 9574–9587.
21. Groot, R. D. Electrostatic Interactions in Dissipative Particle Dynamics Simulation of Polyelectrolytes and Anionic Surfactants. *J. Chem. Phys.* **2003**, *115*, 11265–11277.
22. Vattulainen, I.; Karttunen, M.; Besold, G.; Polson, J. M. Integration Schemes for Dissipative Particle Dynamics Simulations: From Softly Interacting Systems towards Hybrid Models. *J. Chem. Phys.* **2002**, *116*, 3967–3979.
23. Huang, H. W.; Chen, F.-Y.; Lee, M.-T. Molecular Mechanism of Peptide-Induced Pores in Membranes. *Phys. Rev. Lett.* **2004**, *92*, 198304.